Electronic Supplementary Material (ESI) for Journal of Materials Chemistry A.
This journal is © The Royal Society of Chemistry 2023

An isolated Bimetallic Fe-Ru Single-atom Catalyst for Efficient Electrochemical Nitrogen Reduction

*Mengdi Liu, Sai Zhang, Min Chen, Shuxue Zhou, Limin Wu**

Department of Materials Science and State Key Laboratory of Molecular Engineering of Polymers, Fudan University, Shanghai, 200433, China

Corresponding E-mail: lmw@fudan.edu.cn

Chemicals: Zinc acetated dihydrate ($Zn(CH_3COO)_2{\cdot}2H_2O$, 99%), iron acetylacetonate ($Fe(C_5H_7O_2)_3$, 99.9%), potassium hydroxide (KOH, 99%), hydrazine ($NH_2NH_2 \cdot H_2O$, 24-26% in H_2O) ammonia chloride (NH_4Cl, 99.998%), Nafion perfluorinated resin solution (5 wt% in lower aliphatic alcohols and water, contains 15–20% water) and urea ($NH(CO)_2$, 99%) were purchased from Sigma-Aldrich. 2,5-dihydroxyterephthalic acid ($C_8H_6O_6$, 98%), sodium sulphate (Na_2SO_4, 99%), sodium nitroferricyanide ($Na_2[Fe(CN)_5NO]$ $2H_2O$, 99.98%) were purchased from Aladdin Industrial Corporation. Sodium hypochlorite (NaClO, 5% available chlorine), p-dimethylaminobenzaldehyde ($C_9H_{11}NO$, 98%), N-(1-naphthyl) ethylenediamine dihydrochloride ($C_{12}H_{14}N_2$, 98%) and *p*-aminobenzenesulfonamide ($C_6H_8N_2O_2S$, 99%) were purchased from J&K Scientific. Dimethyl sulfoxide-d6 (DMSO-*d*6) was purchased from Cambridge Isotope Laboratories. Inc. Ruthenium acetylacetonate ($Ru(C_5H_7O_2)_3$, 99%) was purchased from STREM chemical. Inc. Salicylic acid ($C_7H_6O_3$, 99.5%) was purchased from Macklin Biochemical Technology Co., Ltd.

Computational details: All the spin-polarized calculations are performed in the framework of the density functional theory with the projector augmented plane-wave method, as implemented in the Vienna ab initio simulation package.[1] The nuclei-electron and the electron exchange correlation interactions were described by the projector augmented wave (PAW) potentials and the generalized gradient approximation (GGA) with the Perdew-Burke Ernzerh of (PBE) functional, respectively.[2-4] The cut-off energy for plane wave is set to 400 eV. The energy criterion is set to 10^{-5} eV in iterative solution of the Kohn-Sham equation. A vacuum layer of 15 Å is added perpendicular to the sheet to avoid artificial interaction between periodic images. The Brillouin zone integration is performed using a 2x2x1 k-mesh. All the structures are relaxed until the residual forces on the atoms have declined to less than 0.03 eV/Å. A semi-empirical van der Waals (vdW) correction proposed by Grimme (DFT-D3) was included to account for the dispersion interactions.[5]

The adsorption energies (ΔG) were obtained by

$$\Delta G = \Delta E_{DFT} + \Delta ZPE - T\Delta S \qquad (1)$$

where ΔE_{DFT} is the reaction energy calculated from DFT; ΔZPE is the zero-point energy; ΔS is the change in entropy.

The formation enegies (E_f) of various models for systems were calculated as follows:

$$E_f = E_{embedded} - E_{pure} + n_C E_C - n_N E_N - n_{Fe} E_{Fe} - n_{Ru} E_{Ru} - n_H E_H \qquad (2)$$

where $E_{embedded}$ and E_{pure} are the total energies of nitrogen-coordinated Ru and/or Fe sites embedded carbon sheets, including the cases of pyridinic-N based, pyrrolic-N-based non-

edged and edged models. The n_CE_C is the reference energy of bulk C system. The n_NE_N, $n_{Fe}E_{Fe}$, $n_{Ru}E_{Ru}$ and n_HE_H are the reference energies of N, Fe, Ru, and H, respectively.

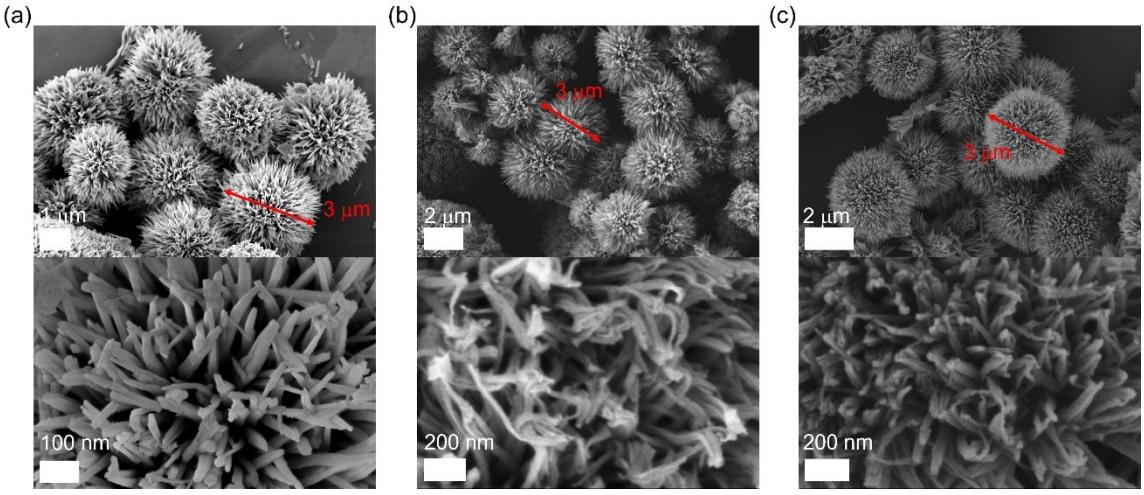

Figure S1. SEM images of a) MOFNR-S, b) CNS and c) FeRu-CNS.

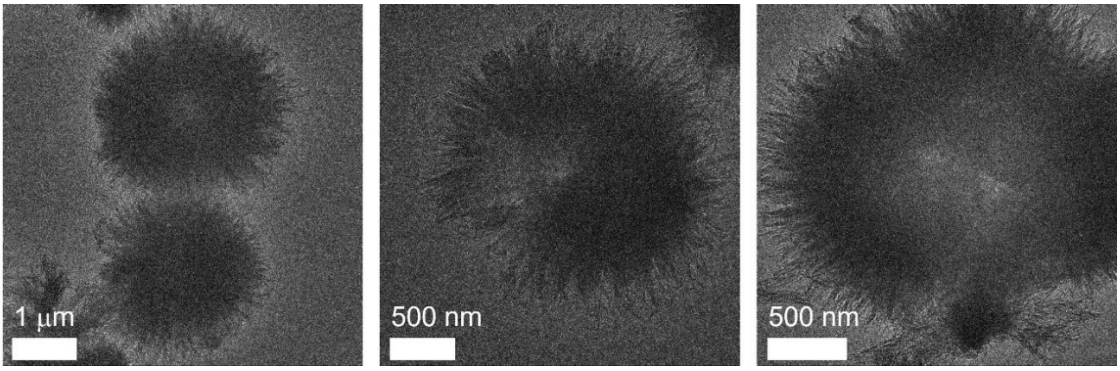

Figure S2. TEM images of FeRu-CNS.

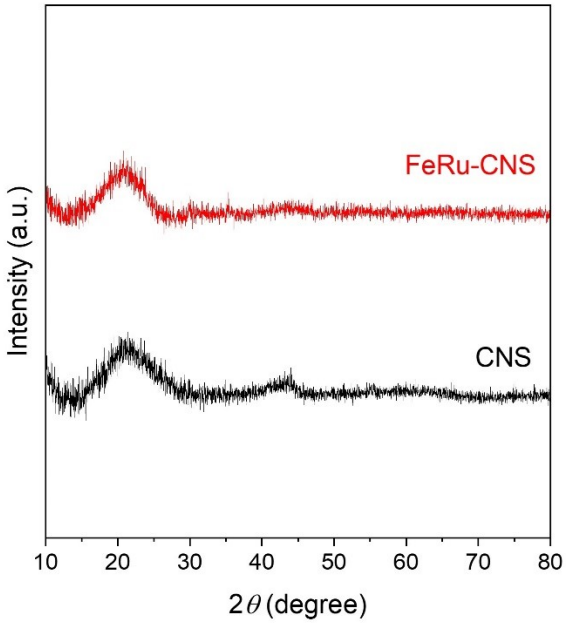

Figure S3. XRD patterns of CNS and FeRu-CNS.

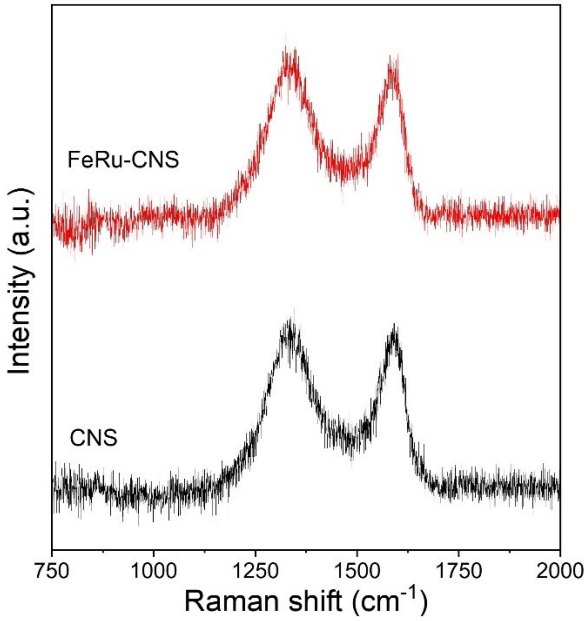

Figure S4. Raman spectrum of CNS and FeRu-CNS.

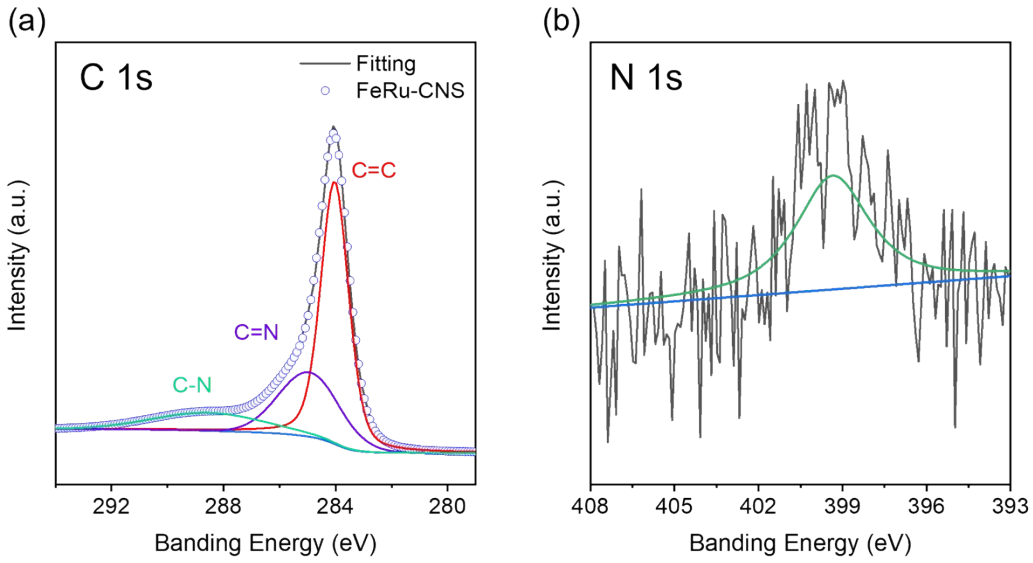

Figure S5. a) C 1s XPS spectra of FeRu-CNS. b) N 1s XPS spectra of FeRu-CNS.

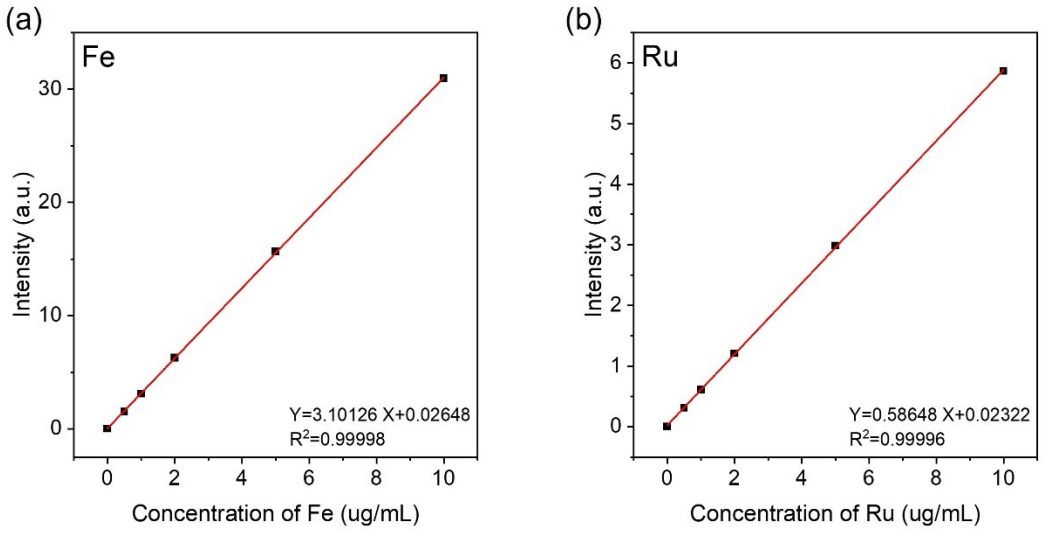

Figure S6. a) Calibration curve of ICP for Fe in FeRu-CNS. b) Calibration curve of ICP for Ru in FeRu-CNS.

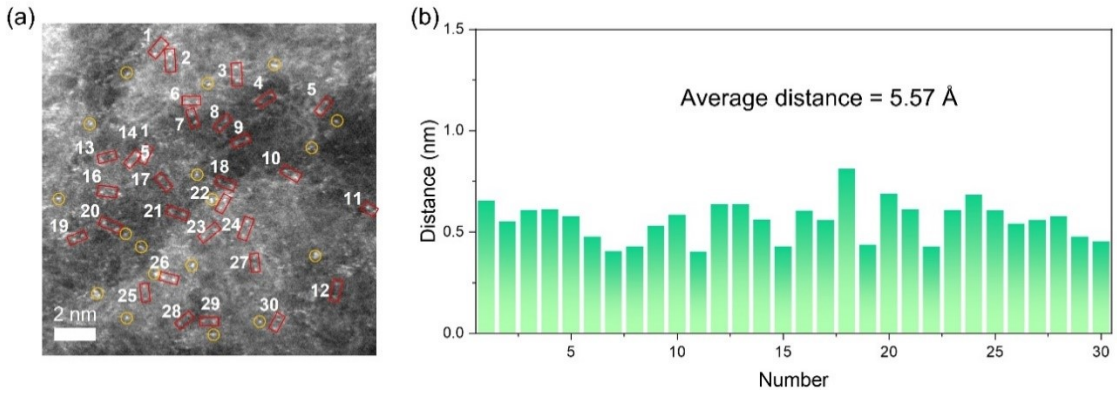

Figure S7. a) HAADF image of FeRu-CNS. Red squares for the isolated single atom pairs, yellow circles for the single atoms. b) Corresponding distribution of distance between isolated single atom pairs in red squares.

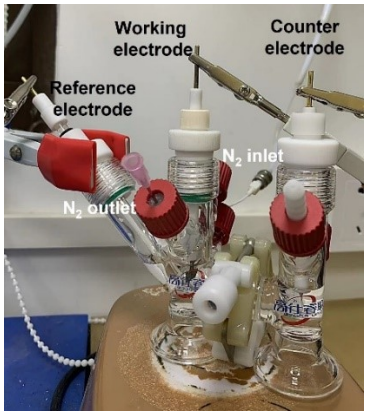

Figure S8. Setup for electrochemical measurement.

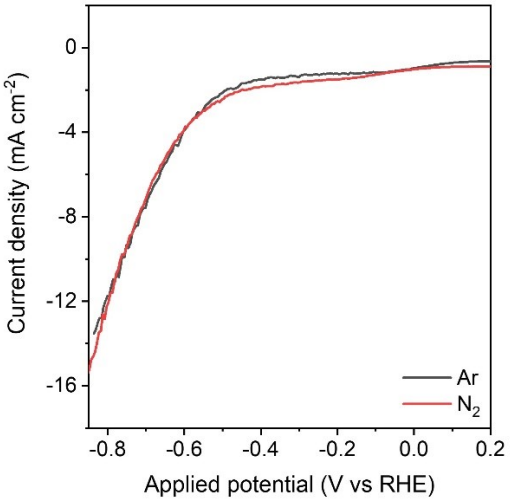

Figure S9. LSV curves of FeRu-CNS in 0.1 M Na_2SO_4.

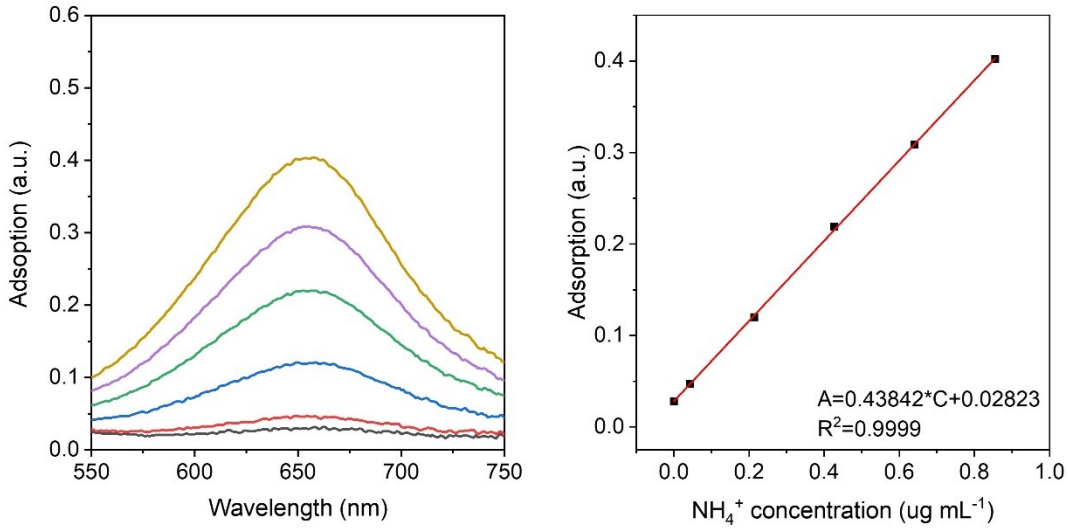

Figure S10. UV-Vis spectrum and Calibration curve for indophenol blue method in 0.1 M Na_2SO_4.

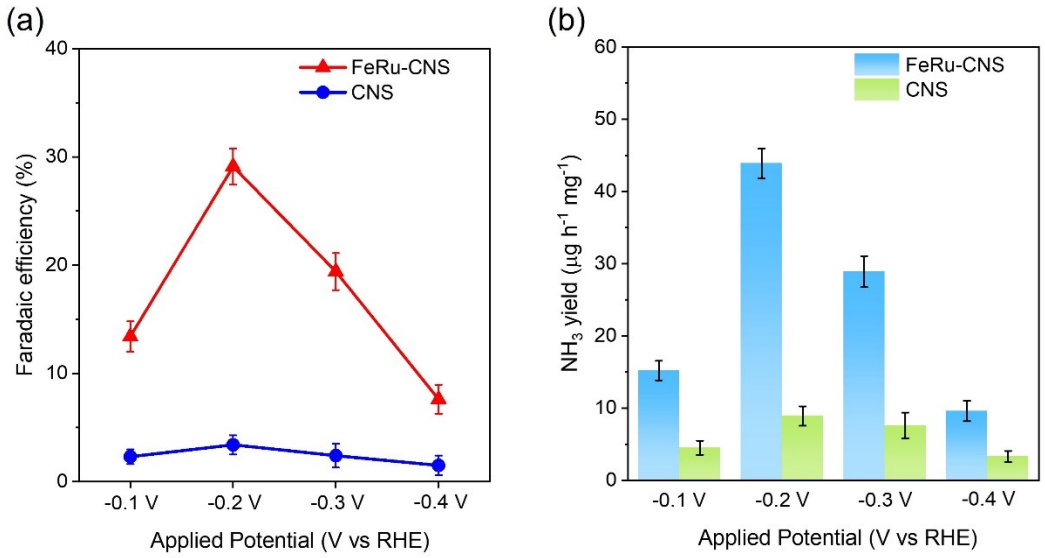

Figure S11. a) Faradaic efficiency of FeRu-CNS and CNS in 0.1 M Na_2SO_4. b) Corresponding NH_3 yield rate of FeRu-CNS and CNS in 0.1 M Na_2SO_4.

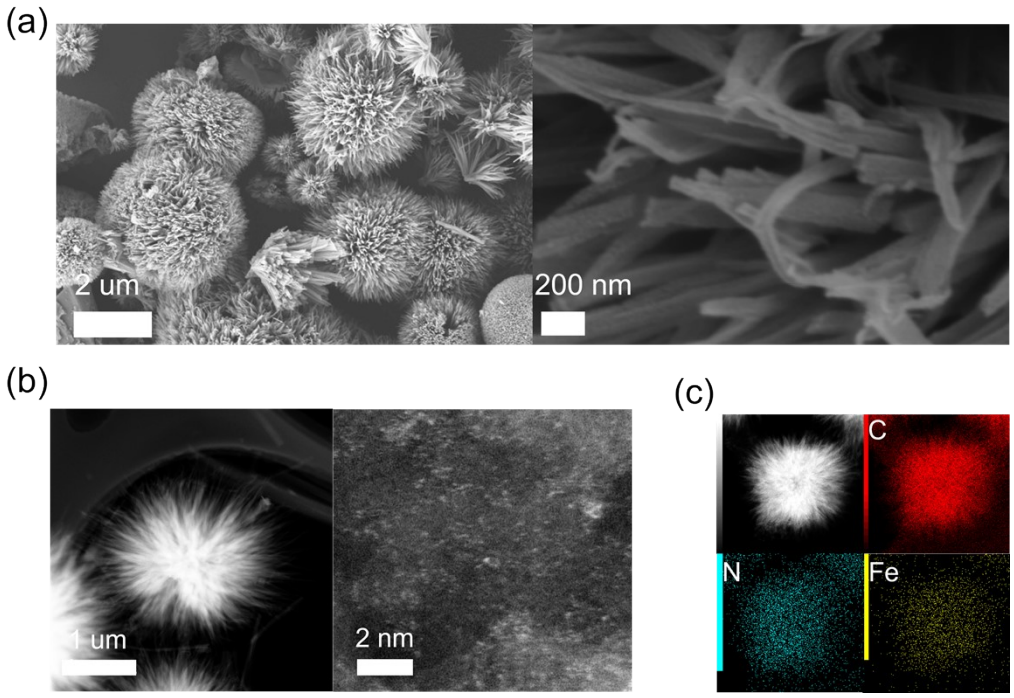

Figure S12. a) SEM images of Fe-CNS. b) HAADF images of Fe-CNS. c) EDS mapping of Fe-CNS.

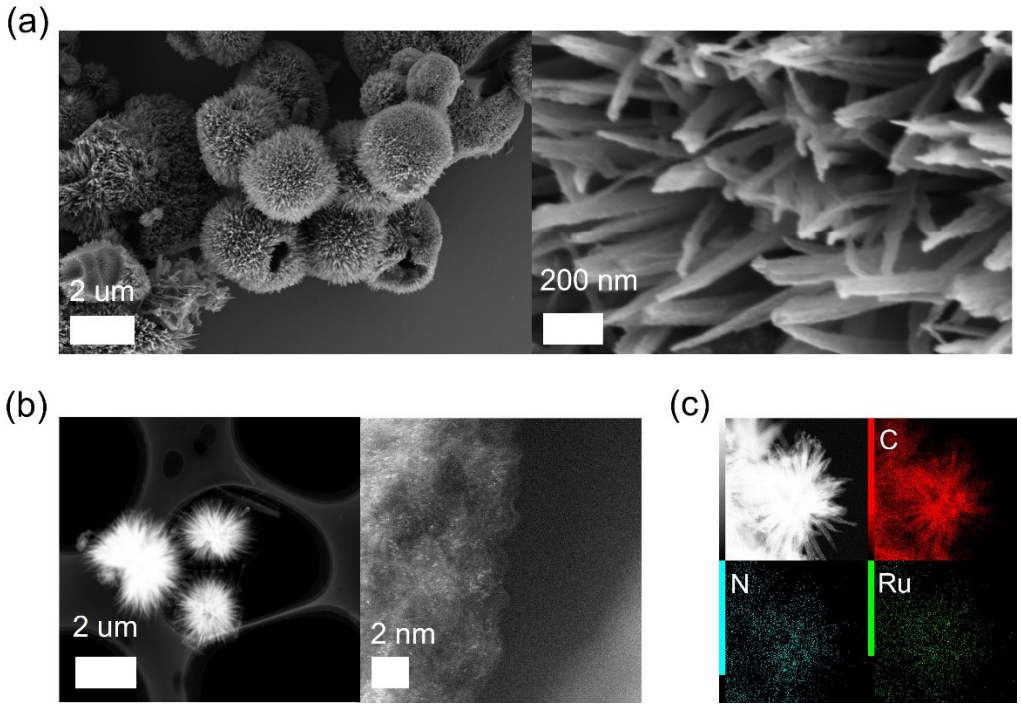

Figure S13. a) SEM images of Ru-CNS. b) HAADF images of Ru-CNS. c) EDS mapping of Ru-CNS.

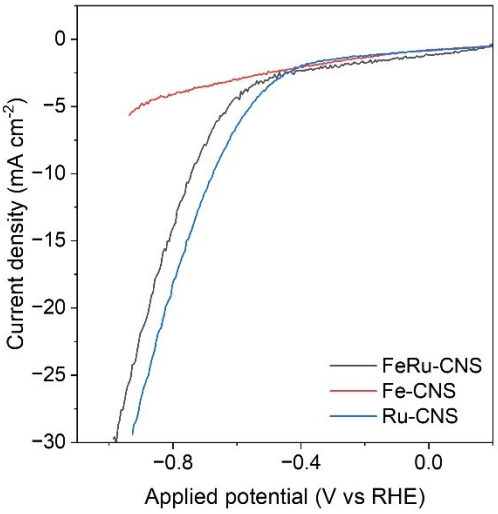

Figure S14. LSV curves of Fe-CNS, Ru-CNS and FeRu-CNS in N_2-saturated 0.1 M Na_2SO_4.

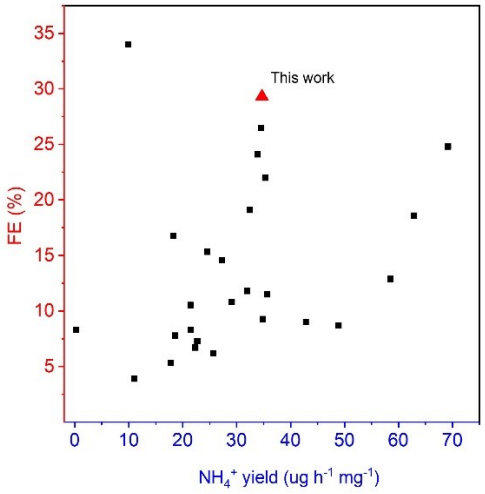

Figure S15. Comparison of electrochemical NRR performance of FeRu-CNS with recently reported Fe-group-based catalysts.

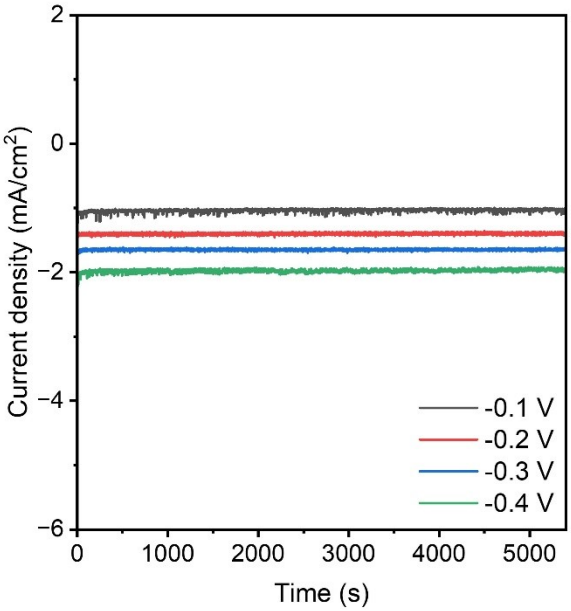

Figure S16. Chronoamperometry curves of FeRu-CNS in 0.1 M Na_2SO_4 under different applied potentials.

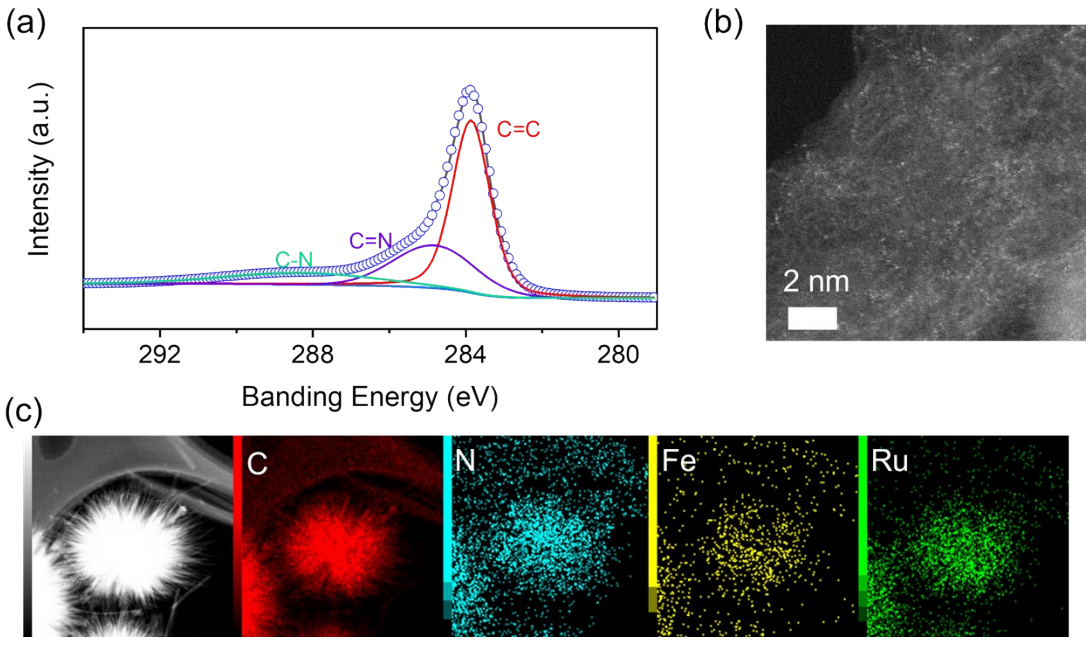

Figure S17. a) C 1s XPS spectra of FeRu-CNS after electrolysis. b) HAADF image of FeRu-CNS after electrolysis. c) EDS mapping of FeRu-CNS after electrolysis.

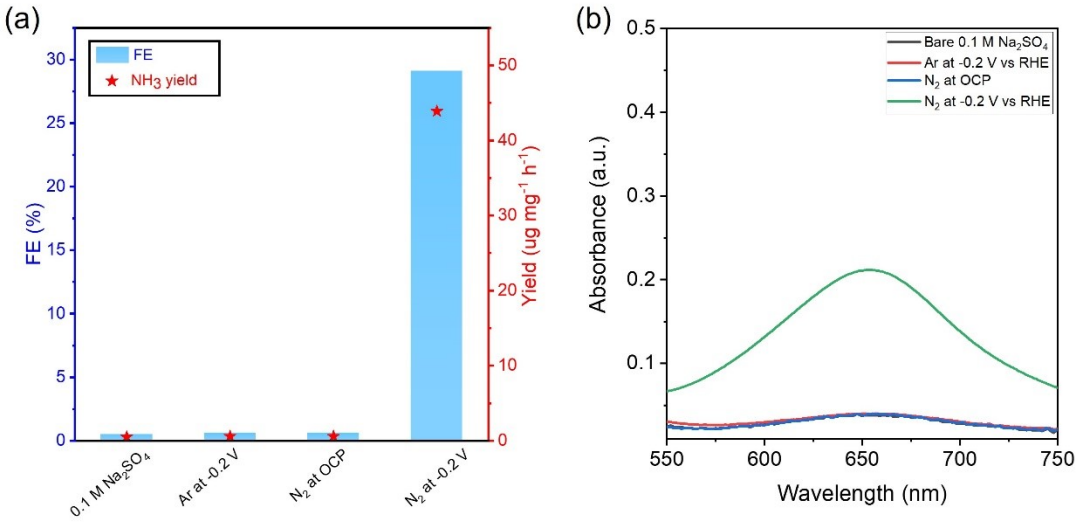

Figure S18. a) FE and NH_3 yield rate of FeRu-CNS under different testing conditions in 0.1 M Na_2SO_4. b) Corresponding UV-Vis adsorption of electrolytes after electrolysis under different EC conditions.

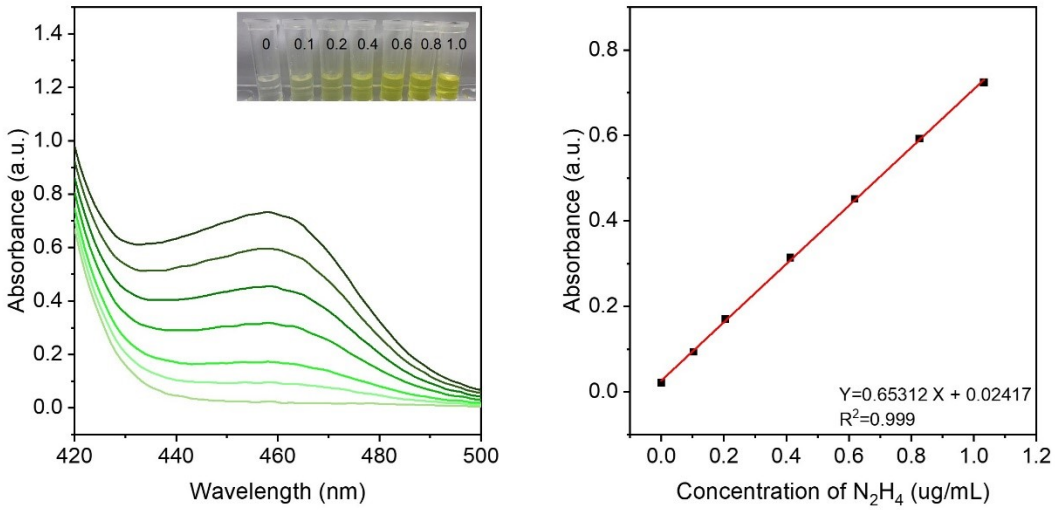

Figure S19. UV-Vis spectrum and Calibration curve for N_2H_4 in 0.1 M Na_2SO_4.

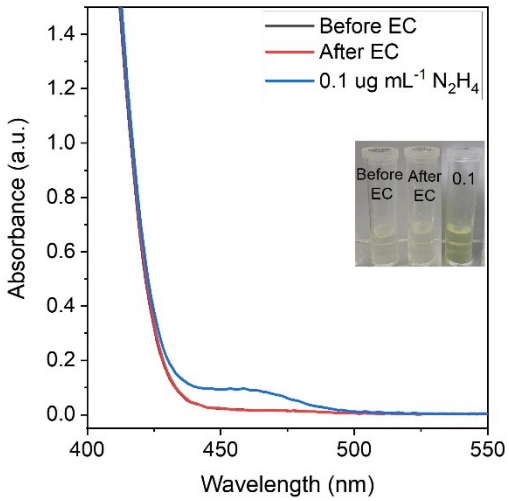

Figure S20. Detection of N_2H_4 before and after electrochemical NRR process.

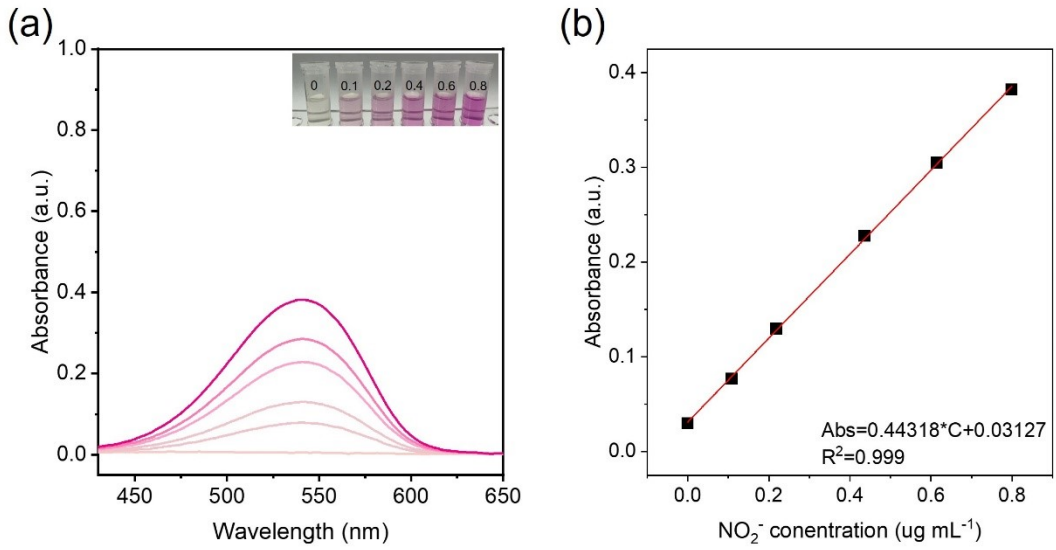

Figure S21. UV-Vis spectrum and Calibration curve for NO_2^- in 0.1 M Na_2SO_4.

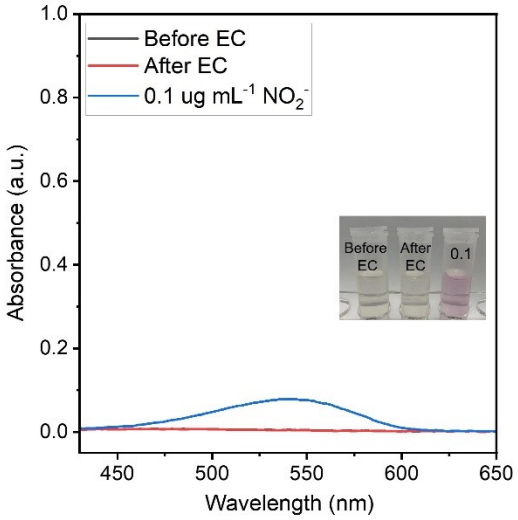

Figure S22. Detection of NO_2^- before and after electrochemical NRR process.

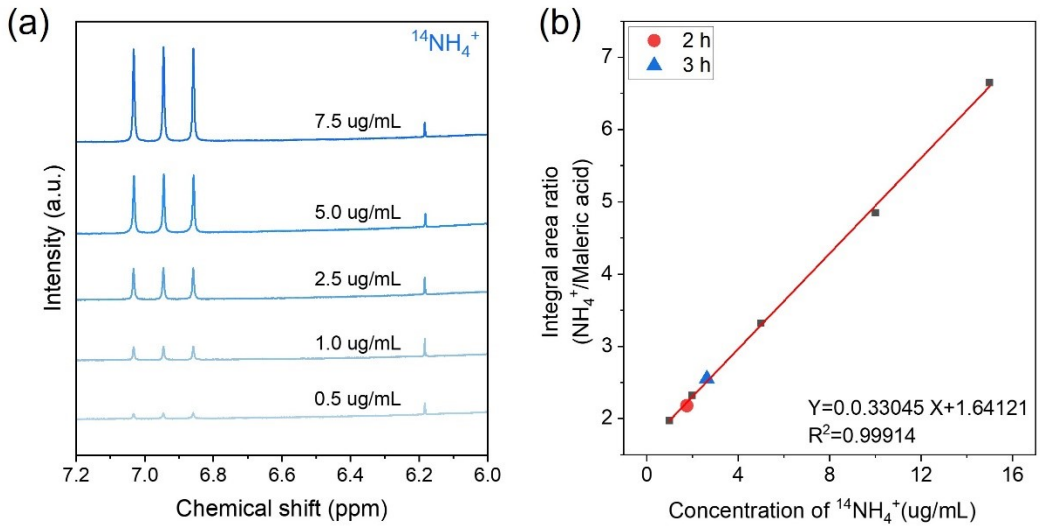

Figure S23. a) ^1H NMR spectrum of $^{14}NH_4^+$ standards. b) Calibration curve of NH_4^+ concentration versus peak area ratio for $^{14}NH_4^+$.

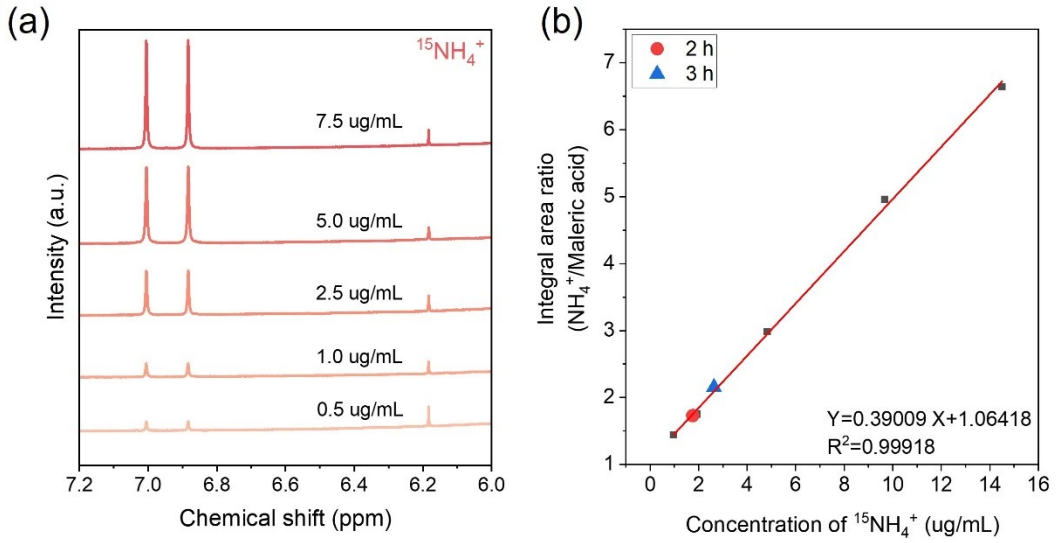

Figure S24. a) ^{1}H NMR spectrum of $^{15}NH_4^+$ standards. b) Calibration curve of NH_4^+ concentration versus peak area ratio for $^{15}NH_4^+$.

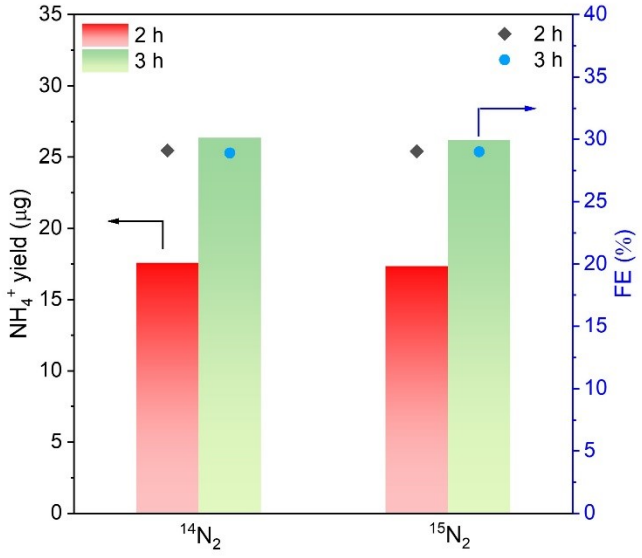

Figure S25. NRR ammonia yield and corresponding Faradaic efficiency measured by NMR using both $^{14}N_2$ and $^{15}N_2$ as feeding gas. Columns for NH_4^+ yield, dots for FE.

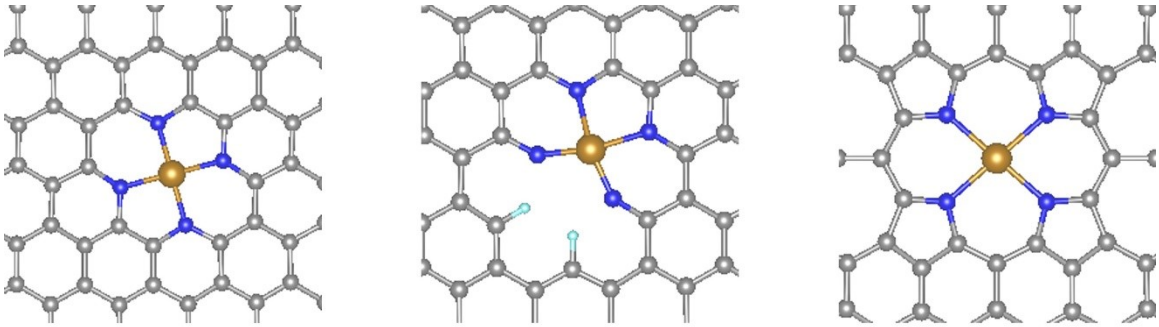

Figure S26. Possible configuration of FeN_4 content and corresponding formation energy. Gray sphere for carbon, blue sphere for nitrogen, gold sphere for iron, light blue sphere for hydrogen.

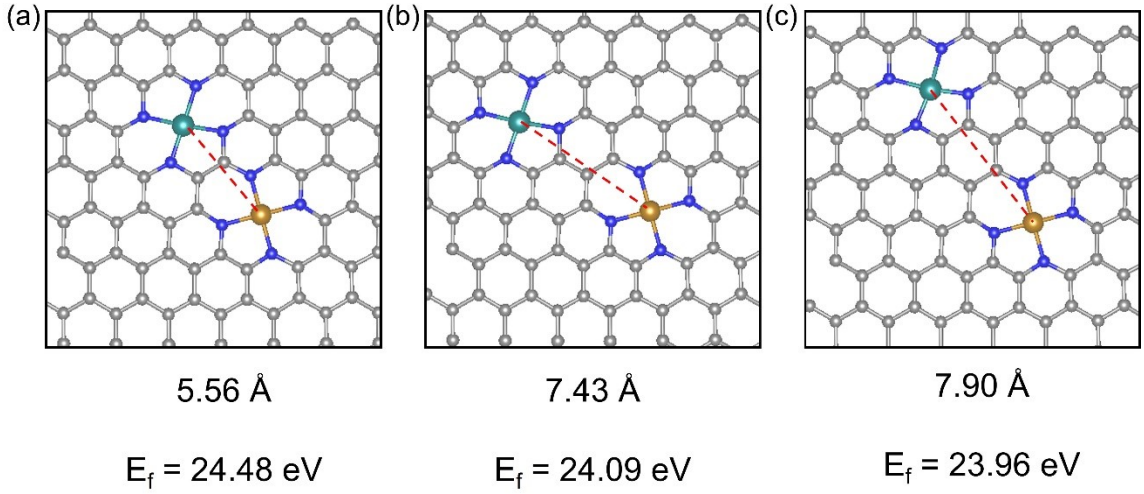

Figure S27. a-c) Possible configuration of FeRu and corresponding formation energy and distance between Fe and Ru atom. Gray sphere for carbon, blue sphere for nitrogen, gold sphere for iron, green sphere for ruthenium.

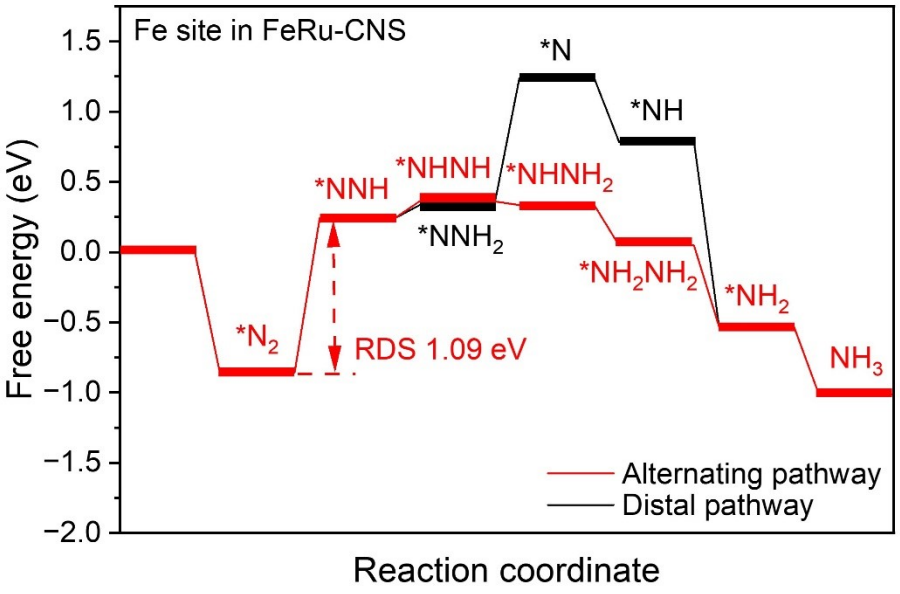

Figure S28. Free energy diagram of nitrogen reduction on Fe site in FeRu-CNS.

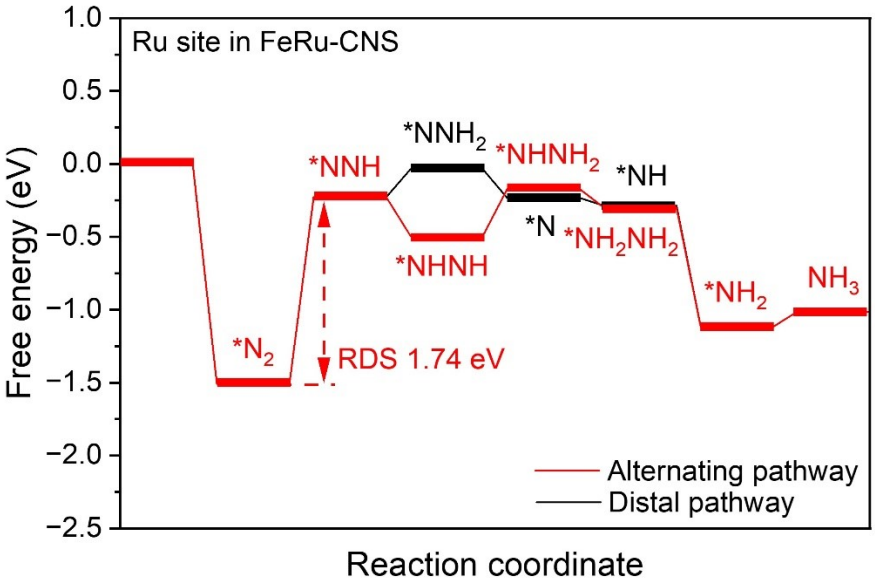

Figure S29. Free energy diagram of nitrogen reduction on Ru site in FeRu-CNS.

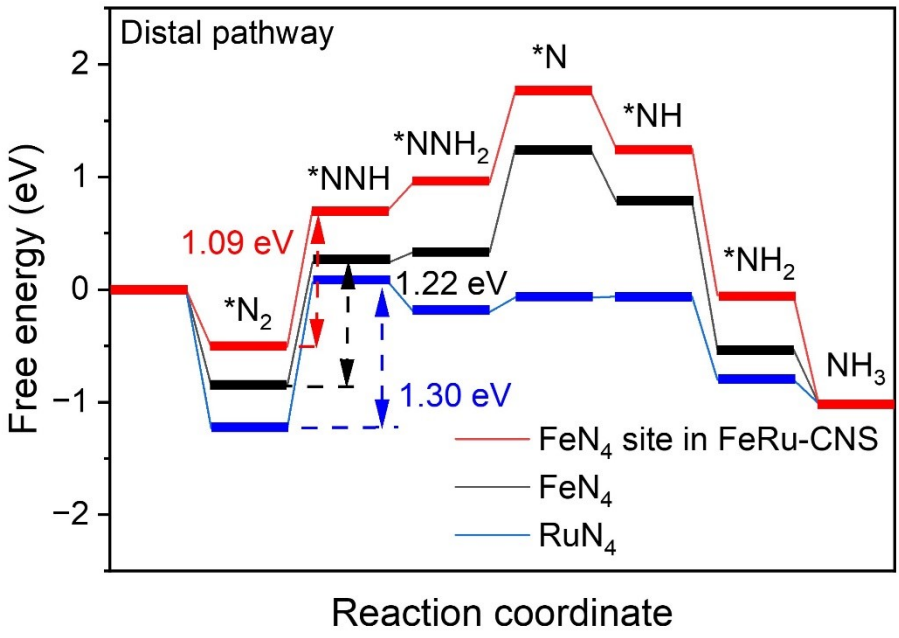

Figure S30. Free energy diagram of distal pathway for nitrogen reduction on FeN_4, RuN_4 and FeN_4 in FeRu-CNS.

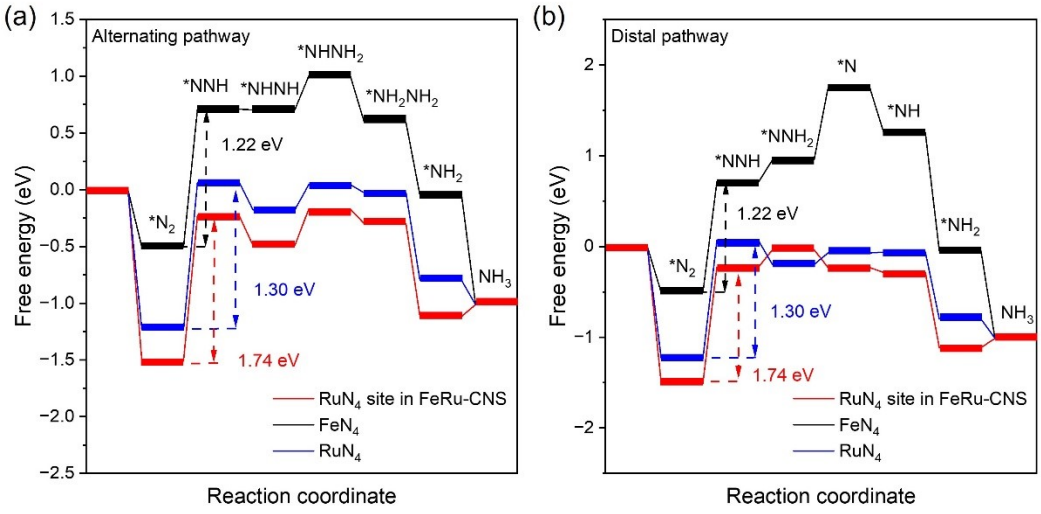

Figure S31. Free energy diagram of alternating pathway (a) and distal pathway (b) for nitrogen reduction on FeN_4, RuN_4 and RuN_4 in FeRu-CNS.

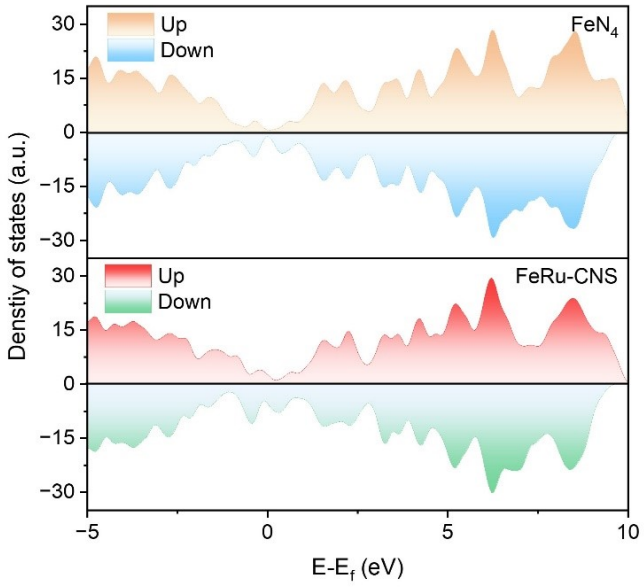

Figure S32. Total density of states of FeN_4 and FeRu-CNS.

Table S1. Determination of Fe and Ru content in FeRu-CNS.

Sample	Mass m_0 (g)	V_0 （mL)	Concentration of samples C_0 (mg/L)	Element	Mass of element C_x（mg/kg)	Wt（%)
1	0.0199	25	4.14	Fe	5214.1	0.52%
2	0.0201	25	4.05	Fe	5422.3	0.54%
3	0.0198	25	4.39	Ru	5234.1	0.52%
4	0.0199	25	4.27	Ru	4992.4	0.50%

Table S2. The Fe K-edge EXAFS curves fitting parameters of FeRu-CNS.

Sample	Shell	*CN*[a]	*R*(Å)[b]	σ^2(Å^2)[c]	ΔE_0(eV)[d]
Fe foil	Fe-Fe	8*	2.455±0.004	0.0034±0.0005	5.2±1.0
	Fe-Fe	6*	2.848±0.007	0.0044±0.0009	
FeO	Fe-O	6.0±0.3	2.120±0.011	0.0138±0.0021	2.2±0.9
	Fe-Fe	11.8±0.5	3.069±0.008	0.0122±0.0010	
FePc	Fe-N	4.0±0.3	1.997±0.012	0.0109±0.0015	5.0±2.3
	Fe-C	6.3±0.6	2.937±0.023	0.0076±0.0014	
Fe_2O_3	Fe-O	6.0±0.3	1.956±0.020	0.0137±0.0021	-8.4±3.0
	Fe-Fe	3.0±0.2	2.946±0.012	0.0106±0.0015	
	Fe-Fe	3.0±0.2	3.380±0.013		
	Fe-Fe	6.0±0.5	3.674±0.013		
FeRu-CNS	Fe-N	3.8±0.6	2.013±0.013	0.0107±0.0020	-0.5±2.1

Table S3. The Ru K-edge EXAFS curves fitting parameters of FeRu-CNS.

Sample	Shell	*CN*[a]	*R*(Å)[b]	σ^2(Å^2)[c]	ΔE_0(eV)[d]
Ru foil	Ru-Ru	12*	2.675±0.003	0.0042±0.0004	-5.8±1.1
$[Ru(bipy)_3]Cl_2$	Ru-N	5.7±0.4	2.07±0.012	0.0021±0.0012	-1.1±0.9
RuO_2	Ru-O	6.0±0.3	2.009±0.013	0.0039±0.0019	-0.1±1.6
	Ru-Ru	2.3±0.2	3.130±0.024	0.0111±0.0012	
	Ru-Ru	7.8±0.5	3.577±0.011		
FeRu-CNS	Ru-N	3.6±0.2	2.024±0.025	0.0066±0.0039	2.8±3.5

Table S4. Comparison of electrochemical NRR performance of FeRu-CNS with recently reported Fe-group-based catalysts.

Catalyst	FE (%)	Yield rate ($ug\ h^{-1}\ mg^{-1}$)	Ref
FeRu-CNS	29.3	43.9	This work
$NiCo_2O_4$@HNCP	5.3	17.8	J.Mater. Chem. A 2020, 8, 1652–1659
CoO QD/rGO	8.3	21.5	J. Mater. Chem. A 2019, 7, 4389–4394
b-FeOOH nanorods	6.7	22.32	Chem. Commun. 2018, 54, 11332–11335.
b-FeO(OH,F) nanorods	9.02	42.84	Chem. Commun. 2019, 55, 3987–3990.
FeOOH QDs-GS	14.6	27.3	Nano Res. 2020, 13, 209–214.
Fe/Fe_3O_4	8.29	0.19	ACS Catal. 2018, 8, 9312–9319.
FePc/C	10.5	137.95	ACS Catal. 2019, 9, 7311–7317.
ISAS-Fe/NC	18.6	62.9	Nano Energy 2019, 61, 420–427.
FeP_2-rGO	21.99	35.29	Chem. Commun. 2020, 56, 731–734.
CoP/CNS	8.7	48.9	Chem. Commun. 2019, 55, 12376–12379.
NiO/G	7.8	18.6	ACS Appl. Energy Mater. 2019, 2, 2288–2295.
P-NiO/CC	10.8	29.1	Inorg. Chem. Front. 2020, 7, 455–463.
N-NiO/CC	7.3	22.7	ChemCatChem 2019, 11, 4529–4536.
Cu NPS-rGO	15.32	24.58	J. Power Sources 2020, 448, 227417.
CuO/rGO	3.9	11.01	ChemCatChem 2019, 11, 1441–1447.
Cu-doped CeO_2	19.1	32.44	Chem. Commun. 2019, 55, 2952–2955.
Fe-Cu clusters	34	9.9	Adv. Mater. 2020, 32, 2004382.
$CoFe_2O_4$/rGO	6.2	25.7	Chem. Commun. 2019, 55, 12184–12187.
NiCoS/C	12.9	58.5	J. Mater. Chem. A 2020, 8, 543–547.
Fe_{SA}-N/CNT	9.28	34.83	ACS Catal. 2019, 9, 336-344.
Fe_{SA}-TPPCl	16.76	18.28	Appl. Catal. B Environ. 2021, 285, 119794.
Fe_{SA}-NO-C	11.8	31.9	Angew. Chem., Int. Ed. 2021, 60, 9078–9085.
PdCu/C-350	11.5	35.7	Angew. Chem., Int. Ed. 2020, 59, 2649–2653.
CuAu@Cu	24.1	33.9	Appl. Catal. B Environ. 2021, 288, 119999.
Pd_{SA}-Cu	24.8	69.2	Angew. Chem. Int. Ed. 2020, 59, 2-8.
Au-Fe_3O_4	10.54	21.42	Adv. Funct. Mater. 2020, 30, 1906579.
Au_{25}-Cys-Mo	26.5	34.5	Small. 2021, 17, 2100372.

Table S5. Bader charge states of Fe and N atoms in FeN_4 site in FeRu-CNS after N_2 adsorption, and Bader charge states of Ru and N atoms in RuN_4 in FeRu-CNS after N_2 adsorption.

	N_2 on Fe site in FeRu-CNS		N_2 on Ru site in FeRu-CNS	
Atom	Fe	N_2	Ru	N_2
Lost |e|	1.19	-	1.31	-
Obtained |e|	-	0.27	-	0.32

Table S6. d-band center of Fe atoms in FeN_4 and FeRu-CNS.

Atom	d-band center (up)	d-band center (down)	d-band center (average)
Fe in FeN_4	-1.835	-0.128	-0.989
Fe in FeRu-CNS	-1.742	-0.067	-0.914

Table S7. Gibbs free energy (eV) for DFT calculations of NRR on FeN_4 in FeRu-CNS.

	E(DFT)	E(cor)	E(system)	E
slab	-1.01E+03	0	-1006.51	0
slab-N_2	-1.02E+03	0.144981	-1023.9	-0.85468
slab-N_2H	-1.03E+03	0.350259	-1026.21	0.240373
slab-NNH_2	-1.03E+03	0.732552	-1029.52	0.334142
slab-N	-1.01E+03	0.055844	-1013.54	1.238062
slab-NH	-1.02E+03	0.270773	-1017.4	0.782668
slab-NH_2	-1.02E+03	0.604572	-1022.11	-0.53016
slab-NH_3	-1.01E+03	0	-1006.51	-1.01235
slab	-1.01E+03	0	-1006.51	0
slab-N_2	-1.02E+03	0.144981	-1023.9	-0.85468
slab-N_2H	-1.03E+03	0.350259	-1026.21	0.240373
slab-NHNH	-1.03E+03	0.731335	-1029.49	0.361925
slab-$NHNH_2$	-1.03E+03	1.040159	-1032.92	0.335526
slab-NH_2NH_2	-1.04E+03	1.41683	-1036.61	0.046874
slab-NH_2	-1.02E+03	0.604572	-1022.11	-0.53016
slab-NH_3	-1.01E+03	0	-1006.51	-1.01235

Table S8. Gibbs free energy (eV) for DFT calculations of NRR on bare FeN_4 site.

	E(DFT)	E(cor)	E(system)	E
slab	-1022.7549	0	-1022.75	0
slab-N_2	-1039.9491	0.156114	-1039.79	-0.50725
slab-N_2H	-1042.3589	0.379385	-1041.98	0.710299
slab-NNH_2	-1045.8737	0.734948	-1045.14	0.955138
slab-N	-1029.3266	0.056221	-1029.27	1.749939
slab-NH	-1033.457	0.285986	-1033.17	1.253381
slab-NH_2	-1038.4771	0.599846	-1037.88	-0.04878
slab-NH_3	-1022.7549	0	-1022.75	-1.01235
slab	-1022.7549	0	-1022.75	0
slab-N_2	-1039.9491	0.156114	-1039.79	-0.50725
slab-N_2H	-1042.3589	0.379385	-1041.98	0.710299
slab-NHNH	-1046.1282	0.737198	-1045.39	0.702888
slab-$NHNH_2$	-1049.5419	1.04512	-1048.5	1.001187
slab-NH_2NH_2	-1053.6905	1.380709	-1052.31	0.592253
slab-NH_2	-1038.4771	0.599846	-1037.88	-0.04878
slab-NH_3	-1022.7549	0	-1022.75	-1.01235

Table S9. Gibbs free energy (eV) for DFT calculations of NRR on RuN_4 in FeRu-CNS.

	E(DFT)	E(cor)	E(system)	E
slab	-1.01E+03	0	-1006.51	0
slab-N_2	-1.02E+03	0.139277	-1024.55	-1.50859
slab-N_2H	-1.03E+03	0.377445	-1026.67	-0.22734
slab-NNH_2	-1.03E+03	0.732113	-1029.89	-0.0371
slab-N	-1.02E+03	0.063718	-1015.01	-0.23336
slab-NH	-1.02E+03	0.319987	-1018.47	-0.28622
slab-NH_2	-1.02E+03	0.585042	-1022.7	-1.11639
slab-NH_3	-1.01E+03	0	-1006.51	-1.01235
slab	-1.01E+03	0	-1006.51	0
slab-N_2	-1.02E+03	0.139277	-1024.55	-1.50859
slab-N_2H	-1.03E+03	0.377445	-1026.67	-0.22734
slab-NHNH	-1.03E+03	0.748262	-1030.34	-0.49225
slab-$NHNH_2$	-1.03E+03	1.029135	-1033.43	-0.1723
slab-NH_2NH_2	-1.04E+03	1.378028	-1036.96	-0.29933
slab-NH_2	-1.02E+03	0.585042	-1022.7	-1.11639
slab-NH_3	-1.01E+03	0	-1006.51	-1.01235

Table S10. Gibbs free energy (eV) for DFT calculations of NRR on bare RuN_4 site.

	E(DFT)	E(cor)	E(system)	E
slab	-1021.7791	0	-1021.78	0
slab-N_2	-1039.6757	0.131746	-1039.54	-1.23402
slab-N_2H	-1042.0513	0.402205	-1041.65	0.064919
slab-NNH_2	-1046.0295	0.713048	-1045.32	-0.19836
slab-N	-1030.1817	0.066458	-1030.12	-0.07072
slab-NH	-1.03E+03	0.31181	-1033.51	-0.06249
slab-NH_2	-1.04E+03	0.594889	-1037.65	-0.79944
slab-NH_3	-1021.7791	0	-1021.78	-1.01235
slab	-1021.7791	0	-1021.78	0
slab-N_2	-1039.6757	0.131746	-1039.54	-1.23402
slab-N_2H	-1042.0513	0.402205	-1041.65	0.064919
slab-NHNH	-1.05E+03	0.777568	-1045.3	-0.17774
slab-$NHNH_2$	-1.05E+03	1.044134	-1048.48	0.044301
slab-NH_2NH_2	-1053.3243	1.370909	-1051.95	-0.02715
slab-NH_2	-1.04E+03	0.594889	-1037.65	-0.79944
slab-NH_3	-1021.7791	0	-1021.78	-1.01235

Reference

1. G. Kresse, D. Joubert, *Phys. Rev. B*, 1999, **59**, 1758-177.
2. P.E. Blöchl, *Phys. Rev. B,* 1994, **50**, 17953–17979.
3. J.P. Perdew, K. Burke, M. *Phys. Rev. Lett.,* 1996, **77**, 3865-3868.
4. J.P. Perdew, M. Ernzerhof, *J. Chem. Phys.,* 1996, **105**, 9982–9985.
5. S. Grimme, J. Antony, S. Ehrlich and H. Krieg, *J. Chem. Phys.,* 2010, **132**, 154104.